RESTRICTIONS ON DEEP FLOW ACROSS THE SHELF-BREAK AND THE ROLE OF SUBMARINE CANYONS IN FACILITATING SUCH FLOW

SUSAN E. ALLEN
Department of Earth and Ocean Science, University of British Columbia, 6339 Stores Rd., Vancouver BC V6T1Z4, Canada
E-mail: sallen@eos.ubc.ca

(Received 28 December 2003; Accepted 4 March 2004)

Abstract. The shelf-break acts as a separator between the coastal ocean and the open ocean. Circulation (particularly deep near-bottom flow) is restricted from crossing the bathymetry. Eddies become elongated in the region of the shelf-break restricting exchange. An estimate of the horizontal eddy diffusivity over the shelf-break of less than 10 m^2 s^{-1} is found from a numerical model. Various mechanisms are responsible for the weak cross-isobath flow that does occur. One is the increase of the Rossby number over small-scale topography such as submarine canyons. Along-shore flow (in the direction opposite to Kelvin wave propagation) generates upwelling through submarine canyons. A review of upwelling through submarine canyons is given. The deep cross-shelf flow generated by the canyons is shown to be as significant as the wind-driven upwelling in some regions. Examples for the reduction of flow across the shelf-break and for upwelling through canyons are taken from the West Coast of Vancouver Island.

Keywords: shelf-break, subinertial flow, submarine canyon, topography, upwelling

1. Introduction

Slow, inviscid, rotating flow near the ocean bottom follows the isobaths and thus flow across the shelf-break (Figure 1) is restricted. By "slow flow" we mean both low velocity flow (low Rossby number) and slowly varying flow (low temporal Rossby number ω/f). Inviscid means we are are considering the flow above the bottom Ekman layer. The near-bottom restriction is for a stratified fluid (Hogg, 1973), where bottom topography is only felt a distance fL/N above the bottom. Here ω is the frequency of variation of the flow, f is the Coriolis parameter, L is a typical horizontal length scale and N is the Brunt–Väisäla or buoyancy frequency.

Given all these restrictions we can consider geostrophic, hydrostatic, homogeneous flow. The momentum equations are:

$$fv = \frac{1}{\rho_o}\frac{\partial p}{\partial x} \tag{1a}$$

Surveys in Geophysics **25:** 221–247, 2004.

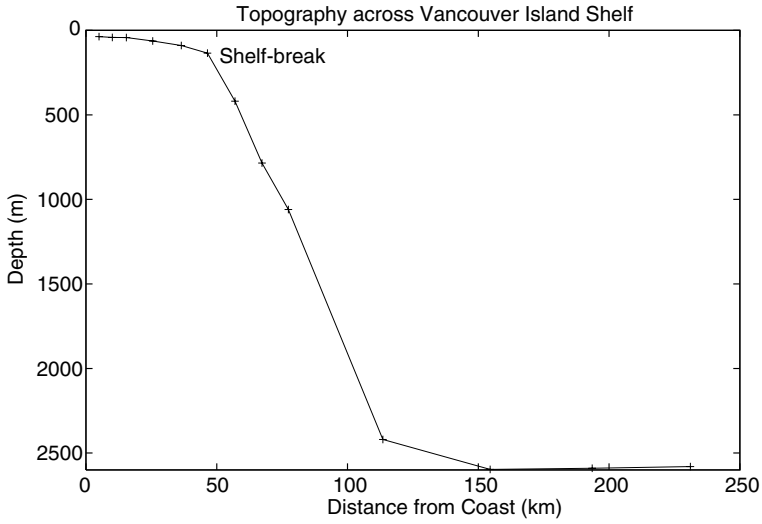

Figure 1. Cross-section of the bathymetry off the West Coast of Vancouver Island, British Columbia. The shelf-break is marked.

$$fu = \frac{-1}{\rho_o}\frac{\partial p}{\partial y} \tag{1b}$$

and the conservation of mass equation is:

$$\frac{\partial}{\partial x}(hu) + \frac{\partial}{\partial y}(hv) = 0 \tag{1c}$$

where (u, v) is the horizontal velocity in the (x, y) directions, respectively, ρ_o is a constant, reference density, p is the pressure and h is the depth (e.g., Cushman-Roisin 1994). If one combines the momentum equations by $\partial/\partial y$ (1a) $-$ $\partial/\partial x$ (1b), one finds the familiar result that geostrophic flow is horizontally divergenceless, e.g., $\partial u/\partial x + \partial v/\partial y = 0$. Substitution into the conservation of mass equation (1c) gives

$$u\frac{\partial h}{\partial x} + v\frac{\partial h}{\partial y} = 0 \quad or \quad \vec{u} \cdot \nabla h = 0 \tag{2}$$

Eq. (2) implies that the flow perpendicular to the isobaths is zero or, in other words, the flow follows the topography. Thus flow is inhibited across steep topographic changes, such as the shelf-break.

1.1. Introduction to canyon effects

There are a large number of mechanisms that can "break" one of the restrictions which force topography-following flow. These mechanisms allow flow to cross the bathymetry. One of these is smaller scale topography leading to large Rossby numbers. For example, consider a very long straight continental shelf and shelf-break. An appropriate Rossby number would be U/fL where L is the width of the shelf. For the Vancouver Island shelf, this width is about 50 km (Figure 1), flow is about $U = 0.4$ m s^{-1} and $f = 1 \times 10^{-4}$ s^{-1} for a Rossby number of 0.08. However, consider a canyon, width 8 km (Figure 2). The Rossby number over the canyon is 0.5 and large enough for advection terms to play a significant role.

We will return to small scale topographic effects and in particular to canyons. However first we will consider the role of the shelf-break in reduced mixing.

1.2. West Coast of Vancouver Island

The Vancouver Island shelf is about 60 km wide to the South and narrows significantly northward toward the block-like Brooks Peninsula (Figure 3). The shelf-break is about 200 m deep. Winds are predominately to the

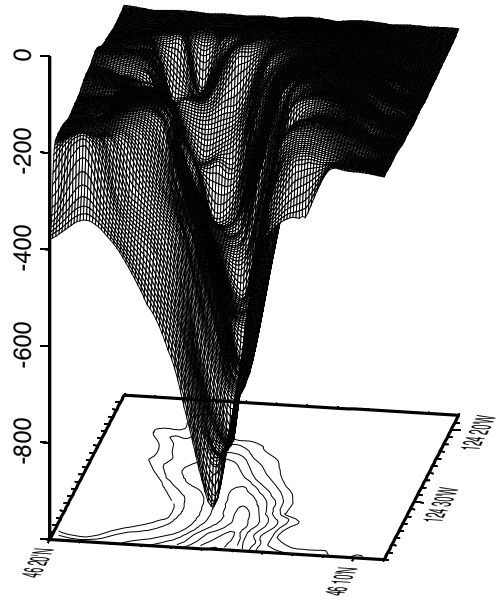

Figure 2. Three-dimensional plot of the bathymetry of Astoria Canyon. (B. Hickey and C. Moore, University of Washington, personal communication).

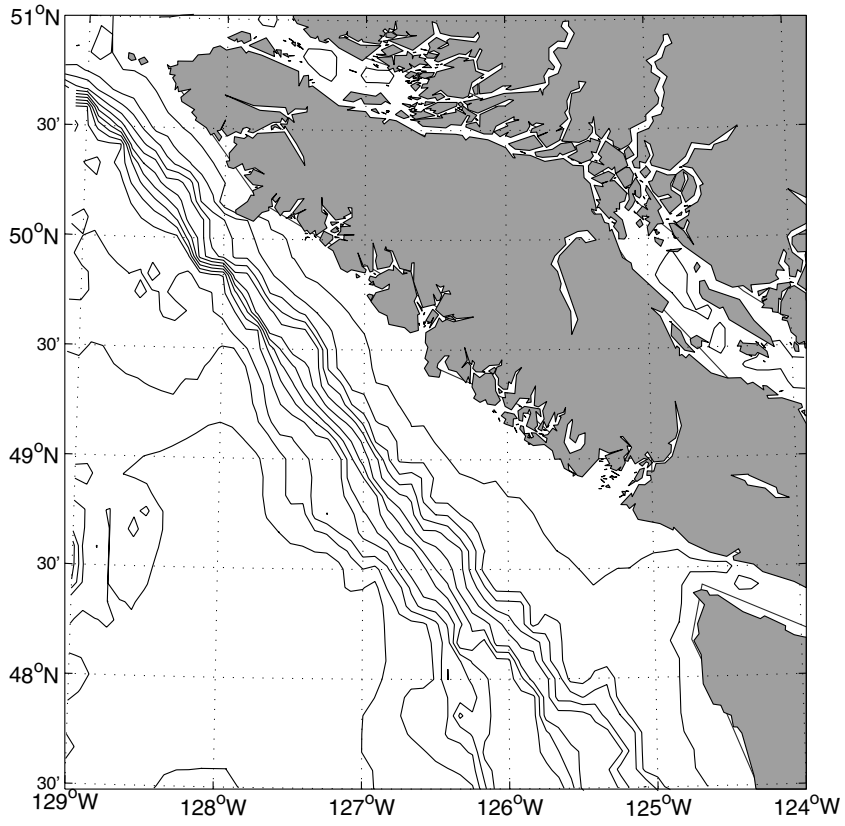

Figure 3. Map showing the coast line and bathymetry off Vancouver Island, British Columbia, Canada. Bathymetric contours 200 m apart. (A. Waterhouse and R. Pawlowicz, University of British Columbia, personal communication).

South in the summer (upwelling-favourable) and to the North in the winter. Rain is common and a large fresh water influx comes from the land. In addition, the Strait of Juan de Fuca is the source of a slightly freshened buoyancy current. This water is formed in the Gulf Islands where the surface plume from the Fraser River is mixed with incoming deep water. This produces slightly freshened, high nutrient surface water which enters the Vancouver Island shelf region at its southern end. The shelf is not straight but cut by numerous submarine canyons, including Juan de Fuca Canyon which cuts the whole shelf and connects the deep open ocean to the Strait of Juan de Fuca.

If one is aboard a vessel off the southern part of the Island one notices quickly the sharp change in the colour of the water as one steams offshore. At about the shelf-break, the water changes from green to blue. Quantitatively, this rapid change from green to blue is due to

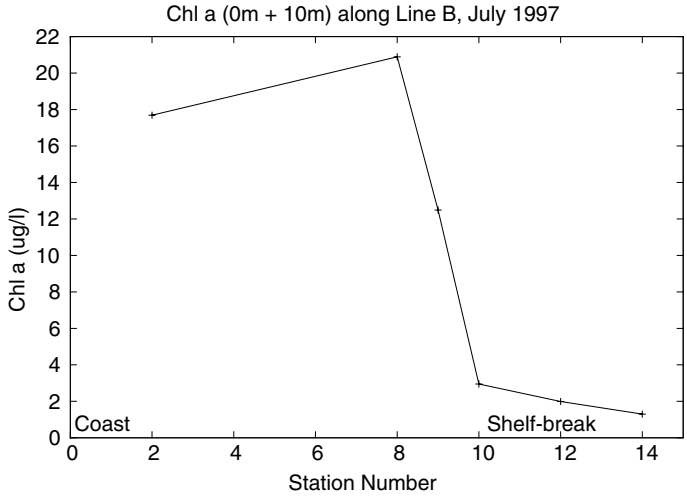

Figure 4. Near surface chlorophyll a along a cross-shelf cruise track. The position of the shelf-break is marked. After Harris (2001).

chlorophyll concentration changes (Figure 4) which are directly related to nutrient changes (Figure 5). Looking carefully at data, one can also determine that there are salinity and temperature changes at this front. However, this is primarily a water property front and is not a density front.

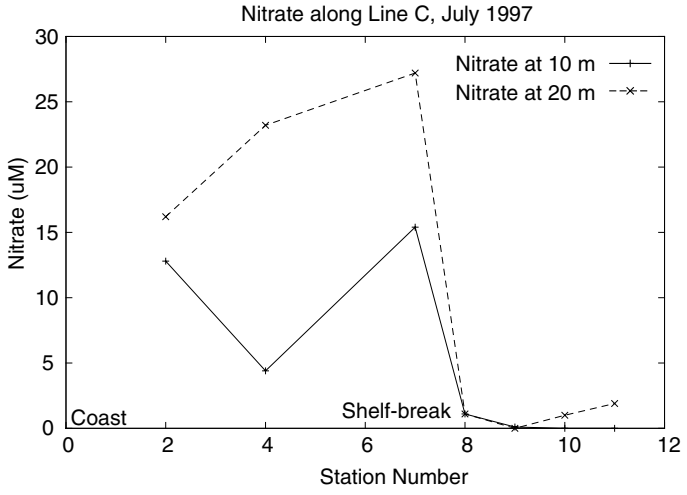

Figure 5. Nitrate at 10 and 20 m along a cross-shelf cruise track. The position of the shelf-break is marked. After Harris (2001).

1.3. Eddies over Topography

How can such a front exist? Why don't eddies mix the water mass contrast?

Eurin (1999) used the results of a simple primitive equation model driven by a stochastic wind field to investigate these questions. The mean topography is composed of three distinct features: the abyssal plain, a steep slope and the continental shelf. The abyssal plain and the continental shelf are assumed to be gently sloping surfaces, with a constant tilt. The in-between slope is a region of increased steepness. Along-shore variations in bathymetry were added over the slope. They are randomly generated and their size is dependent on the square of the mean topography's local slope. The bumps therefore introduce along-shore variability mainly over the slope (Figure 6).

The wind forcing was not designed to represent a realistic wind field but to generate an active eddy field and not have a net force in any direction.

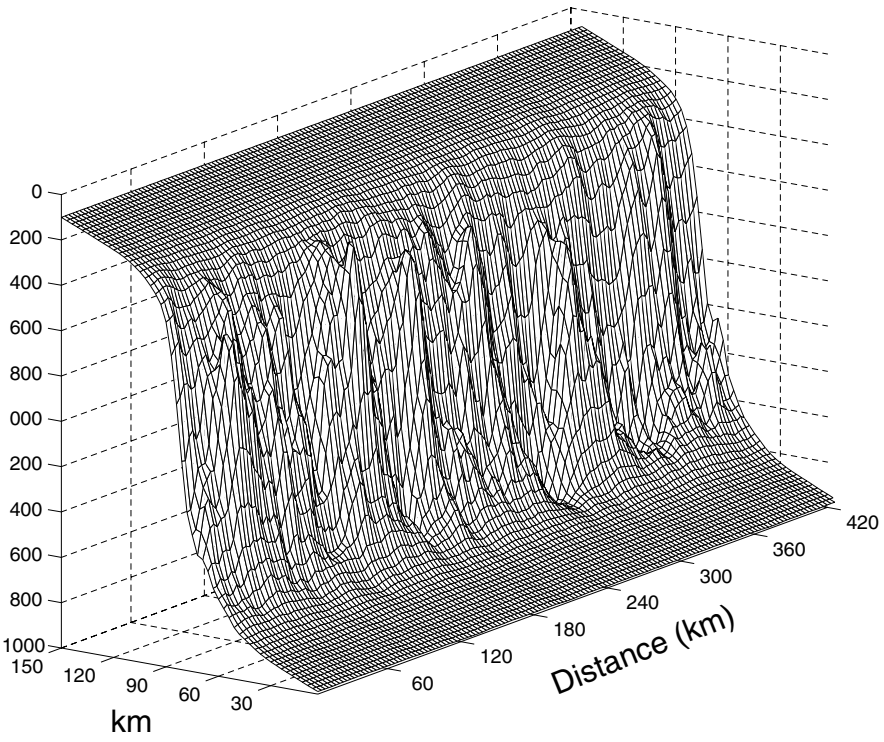

Figure 6. The bathymetry of the slope region showing the topographic bumps. Reprinted with permission from (Eurin, 1999).

It has a time-scale of about three days. The model was run for 250 days. The circulation shows both eddy and mean features. The strongest flows are in the shallow water (Figure 7). A mean current keeping shallow-water the to right (poleward) is observed over the slope. A second mean current in the opposite direction (equatorward) occurs over the shelf. The strongest eddies occur over the shelf and tend to be elongated along-shore.

Eddies are small over the steep-shelf break and tend to (a) be strongly elongated alongshore or (b) be the direct result of the small scale topography. Thus, not only mean flows, but also eddy activity, is inhibited across the bathymetry.

1.4. "Eddy viscosity" over steep topography

So how inhibited is the flow across the topography?

In order to evaluate the eddy-mixing coefficients across the continental slope, Eurin (1999) used a passive scalar. The scalar had value 1 at the coast and value 2 at the ocean boundary. Initially it varied linearly

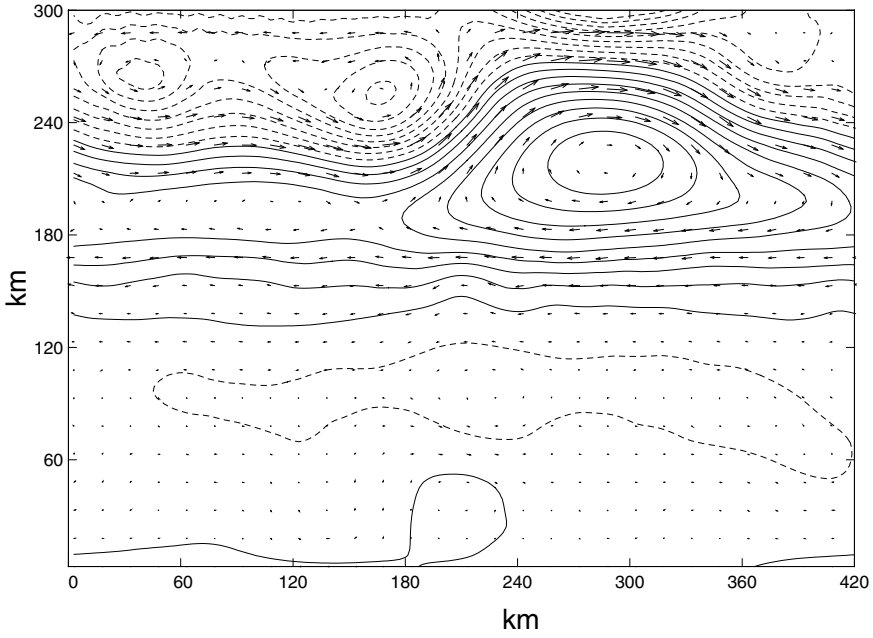

Figure 7. Snapshot of the circulation. The coast is toward the top of the page and the ocean toward the bottom. Solid (dashed) contours are the positive (negative) surface elevation anomaly. (Contour interval 4 m). Only one in five velocity vectors is shown. (r.m.s. velocity 45 cm s^{-1}). Reprinted with permission from (Eurin, 1999).

between the two. The model was run for 250 days and scalar fluxes and concentration gradients were calculated by averaging over the last 100 days.

To correctly estimate the eddy-mixing coefficients it is necessary to obtain the correct transport of the scalar. Unfortunately, numerical advection is not yet a solved problem – every year several papers are published which describe new numerical schemes for the transport equation. Here a Trenback–Bott scheme with a flux-corrected transport (FCT) algorithm was used (Eurin, 1999). The usual FCT had to be modified to take into account layer-thickness changes.

A snapshot of the tracer distribution is shown in Figure 8. Initially the tracer had an even gradient from the ocean to the coast. After 8 months simulation the tracer has been well mixed over the shelf. A strong gradient occurs near the coast where the eddy energy is reduced due to the proximity of the coast. Two strong gradients appear in the shelf region. One is diffuse and meandering and the other is continuous across the domain and sits over the topographic slope.

We approximate the eddy-diffusivity coefficient by assuming the concentration flux is given by: depth $\times$ the eddy-diffusivity $\times$ the along-shore

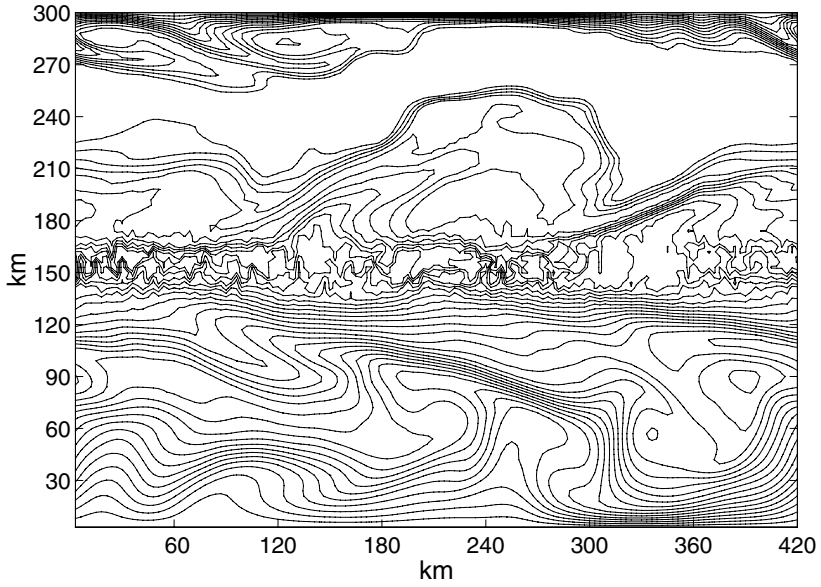

Figure 8. Snapshot view of the passive scalar concentration after 8 months of simulation (contour interval 0.02). Note that the snapshot does not coincide with the circulation figure. Reprinted with permission from (Eurin, 1999).

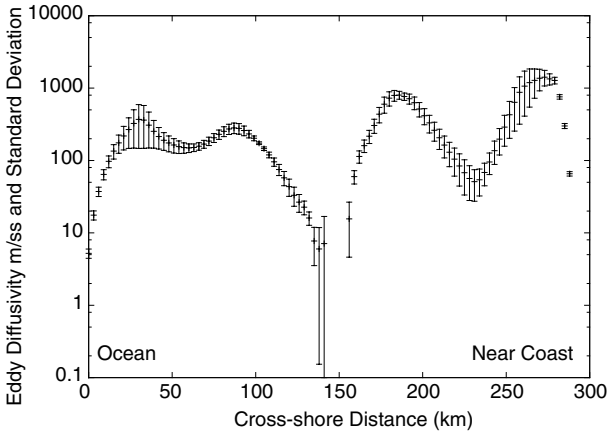

Figure 9. Spatial variations of the eddy-diffusivity coefficients as estimated in units of $m^2\ s^{-1}$. The ocean is on the left-hand side of the plot.

average concentration gradient (Figure 9). The spatial variations of the eddy-diffusivity reflect the observed tracer distributions. Low eddy-diffusivities are seen near both walls and over the slope. The minimum eddy diffusivity occurs near the bottom of the slope. Over the slope the eddy diffusivity is enhanced by the topographic bumps.

Note that the presence of a front does not mean that there is no mixing across it. It simply means that the mixing in the region of the front is reduced compared to the mixing elsewhere. By conservation of tracer, the flux of the tracer offshore is constant across the shelf-slope domain. In the region of the front, the flux is maintained (in the absence of strong mixing) by strong gradients.

1.5. Discussion and extension to stratified flows

The observed eddy-diffusivity is a function of two processes: the distribution of eddy-kinetic energy and the depth gradients (more rigorously the potential vorticity gradient). The depth gradients (potential vorticity gradients) inhibit cross-shelf exchange by causing elongation along-shore of the eddies.

The eddy kinetic energy is strongest over the shelf because the water is shallowest there. Thus the eddy diffusivity is higher over the shelf. The second region of high eddy-kinetic energy is over the slope because of the topographic bumps. At the two boundaries (the coast and the open boundary), the eddy-kinetic energy is reduced (due to the choice in forcing) and the eddy diffusivity is reduced.

The gradient of the topography is largest over the slope and cross-shelf mixing is strongly reduced. There is also reduced mixing over the shelf in the region of an equatorward shelf-jet which has high vorticity.

Fronts, such as those seen off the West Coast of Vancouver Island, may be generated by the eddy field rather than being maintained by the mean flow. The eddy field itself is strongly constrained by potential vorticity gradients, due both to topographic gradients and due to strong jets. The elongation of the eddies in the vicinity of strong potential vorticity gradients inhibits exchange and generates passive scalar fronts.

However, the fronts we see (Figures 4 and 5) are near surface and the flow is stratified. Why do we see the fronts? The lengthscale of the slope is of order 15 km, the buoyancy frequency is 1×10^{-2} s^{-1} and $f = 1.0 \times 10^{-4}$ s^{-1} which would give a scale height of 150 m which is smaller than the depth but is the right order of magnitude. Another possible reason to see the front near the surface is that the deep isopycnals are steeply tilted (due to upwelling, Figure 10). These tilted isopycnals may act like topography to the flow above.

2. Upwelling over short canyons

2.1. An upwelling episode over a short canyon

Consider a straight section of coast with a single canyon. Assume the canyon is 10–20 km across, 10–20 km long and 300–600 m deep and that

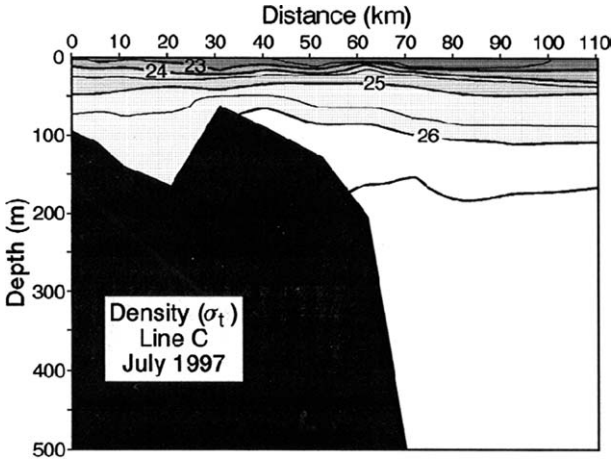

Figure 10. Cross-section of the isopyncals across the Vancouver Island Shelf, July 1997. (R. Thomson, Institute of Ocean Sciences, personal communication.)

it cuts the continental shelf about half-way to the coast. Consider a southward flowing (opposite to the Kelvin wave direction) current over the shelf and shelf-break.

The current will be in geostrophic equilibrium with a cross-shore pressure gradient. Thus the pressure is lower toward the coast. However, within the canyon, the flow cannot be to the South because of the canyon walls. The Coriolis force is zero and so there is an unbalanced pressure gradient. This pressure gradient is the driving force for enhanced upwelling through canyons (Freeland and Denman, 1982).

The flow over a canyon during upwelling has a complicated three-dimensional structure (Figure 11).

(1) Near surface flow is only weakly affected by the canyon and passes directly over the canyon.
(2) Flow just above the depth of the canyon rim (the edge where the near flat shelf meets the steep bathymetry) flows over the upstream rim of the canyon. As it crosses the rim, it flows down into the canyon, stretching the fluid columns and generating cyclonic vorticity. The flow then turns up-canyon and flows across the canyon equatorward, shoreward and upward leaving the canyon shoreward of its original position. As the flow crosses the canyon it decreases its depth and the stretching decreases. As the flow crosses the downstream rim, fluid columns are compressed generating anti-cyclonic vorticity. The stretching can be strong enough to generate a closed cyclonic eddy at this depth (''rim depth eddy'' in Figure 11) (Allen et al., 2001).

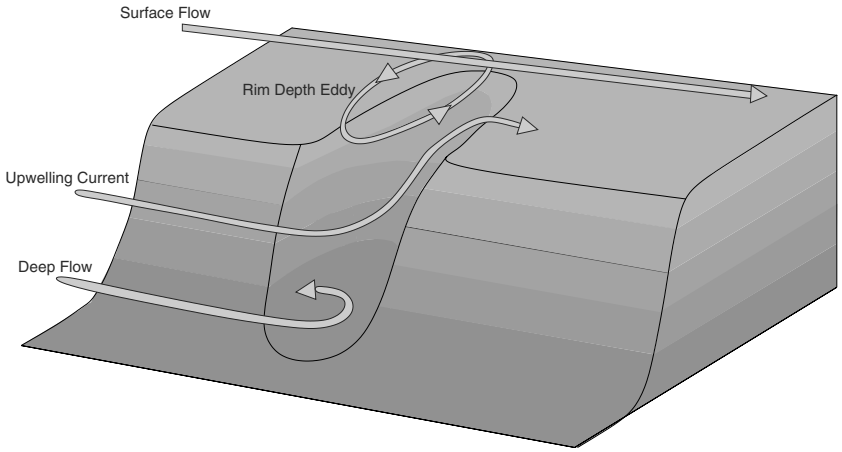

Figure 11. Schematic of the flow over a submarine canyon during upwelling. (After Allen and Hickey, submitted.)

(3) Flow over the slope at the depth of the rim of the canyon and for some depth below ("upwelling current" in Figure 11) is advected into the canyon and upwells over the downstream rim of the canyon near the head. This flow carries the deepest water advected onto the shelf.
(4) The upward vertical displacement of water parcels decreases with depth. Thus water deeper than that which upwells onto the shelf is stretched within the canyon and has cyclonic vorticity ("deep flow" in Figure 11).

2.2. The active layer

Upwelling flow through a canyon is driven by the cross-shelf pressure gradient at the depth of the rim. The pressure field can be modified significantly by the presence of the canyon. For very wide canyons the cross-shelf pressure gradient is modified over the canyon so that the flow can smoothly follow the isobaths. A measure of the ability of the flow to follow the isobaths is given by the Rossby number ($R_o = U/f\mathcal{R}$) based on the ratio of the required acceleration of the flow to turn onshore at the upstream side of the canyon to follow the isobaths ($U^2/\mathcal{R}$ where $\mathcal{R}$ is the turning radius of the shelf-break isobath upstream of the canyon) and the Coriolis force (fU where f is the Coriolis parameter and U is the incoming velocity of the shelf current) (Allen and Hickey, submitted).

For small R_o one can show that flow velocity across the canyon is R_oU and that the pressure gradient along the canyon is $-\rho_o fUR_o$ where ρ_o is a reference density (Allen and Hickey, submitted). The configuration of the active layer flow is shown in Figure 12. Note that in addition a strong eddy can form over the upstream rim. The eddy structure can be considered an addition (superposition) to the illustrated flow.

2.3. The upwelling layer

Now consider the water which passes through the mouth of the canyon and is upwelled onto the shelf. The deepest isopycnal that is upwelled onto the shelf is that one which just touches the rim of the canyon at the canyon head (depth H_h). At the canyon mouth, this isopycnal has depth $Z + H_h$. At this depth there must be a balance in the canyon such that the pressure at the mouth of the canyon is the same as that at the head (Figure 13). The tilted isopycnals provide a baroclinic pressure gradient to balance the pressure gradient at the rim so that below this isopycnal the flow does not go from the canyon up onto the shelf.

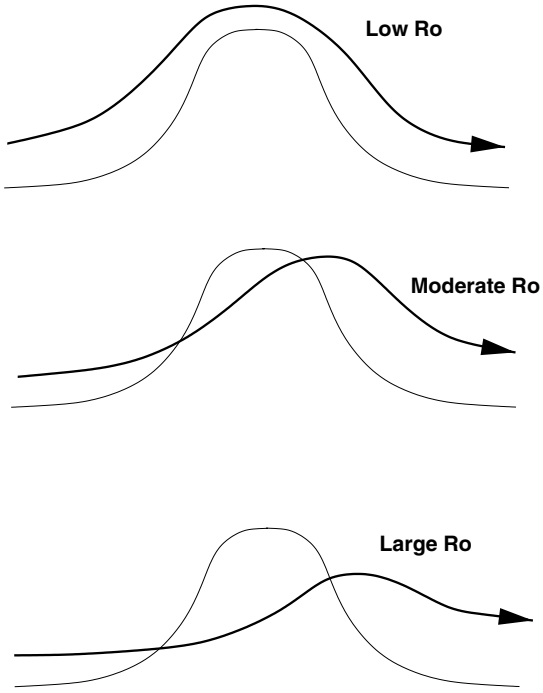

Figure 12. Plan view of the active layer flow for small, moderate and large Rossby numbers. The thin line represents the rim of the canyon.

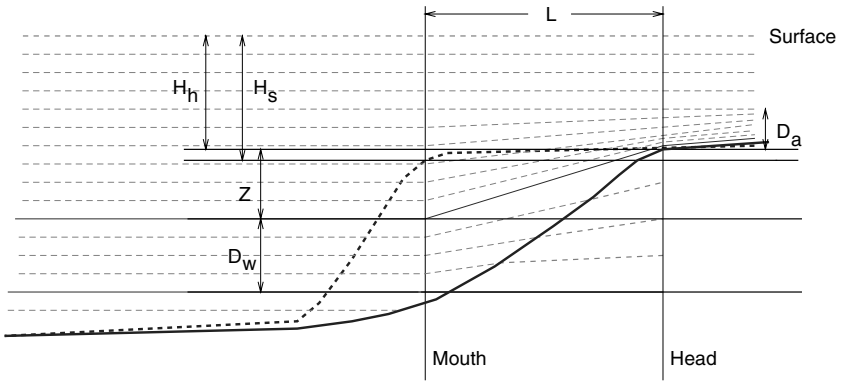

Figure 13. Sketch to illustrate the baroclinic pressure gradient due to isopycnals (fine lines) tilting toward the head of the canyon. The sketch shows a cross-section through the centreline of the canyon. The bottom-topography away from the canyon is given by the bold dashed line. The height Z is determined by balancing the pressure gradient at rim-depth and the change in baroclinic pressure gradient due to the tilted isopycnals. The depth $H_h + Z$ is the deepest water upwelled onto the shelf. The column-stretching deep in the canyon is given by the ratio Z/D_w. (After Allen and Hickey, submitted.)

Scaling and combining the density advection equation, the conservation of mass equation and balancing the pressure, allows us to solve for the depth of upwelling (Allen and Hickey, submitted):

$$Z = \left(\frac{fULR_o}{N^2}\right)^{1/2} \tag{3}$$

Assuming that the cross-stream pressure gradient scales as the rim-depth pressure gradient, one can estimate the velocity of the upwelling stream. For low Rossby number it is UR_o (Allen and Hickey, submitted). The total upwelling flux is the velocity UR_o multiplied by the width W_{sb} and the depth of the upwelling stream Z.

2.4. The deep water

Assuming conservation of potential vorticity, the stretching S of the water column multiplied by the Coriolis frequency gives the deep cyclonic vorticity. The fluid of interest is that below Z to the deepest isopycnal that is significantly elevated within the canyon. If this isopycnal occurs at scale depth D_w below Z at the mouth of the canyon, then the water column that has a length $Z + D_w$ near the head of the canyon has a length D_w at the mouth of the canyon (Figure 13) and $S = Z/D_w$.

Under the deepest isopycnal that upwells through the canyon, the pressure is actually higher at the head of the canyon than at the mouth. This pressure gradient is in balance with the cyclonic circulation at depth. The depth D_w is the depth of penetration, into the canyon, of the effect of the topography at rim depth. Scaling conservation of potential vorticity and the thermal wind equation and combining gives $D_w = fL/N$ where L the length of the canyon has been taken as the eddy length scale (Allen and Hickey, submitted).

2.5. The rim depth eddy

The rim depth flow crosses the upstream canyon edge, feeling the slope of the canyon, down to a depth Z. The thickness of the rim-depth flow D_a does not obey the Hogg Scale NL_e/f as this is larger than the water depth of the shelf (using a combination of the width and length as a scale for L_e). Thus the rim-depth flow thickness must scale with the depth of the water H_s. The stretching of this flow across the canyon is given by Z/H_s which generates a vorticity fZ/H_s.

This cyclonic vorticity has a width given by the half-width of the canyon and is imbedded in a flow of strength U. If the flow velocity generated by the vorticity is equal to the background flow then the total flow will be zero in one region. If the vorticity is stronger than this, closed streamlines will form. Thus the velocity due to the vorticity scales as fZW/H_s (Allen and Hickey, submitted) and an eddy forms if

$$E = \frac{fZW}{UH_s} \tag{4}$$

is large.

The rim-depth eddy over Barkley Canyon was determined using Conductivity–Temperature–Depth (CTD) measurements and a diagnostic numerical model (Figure 14). The eddy is so strong it is hard to see the background flow over the canyon.

Mean eddies can also be generated by oscillatory flow, such as tides, over submarine canyons (Boyer et al., 2000). The generation of a mean

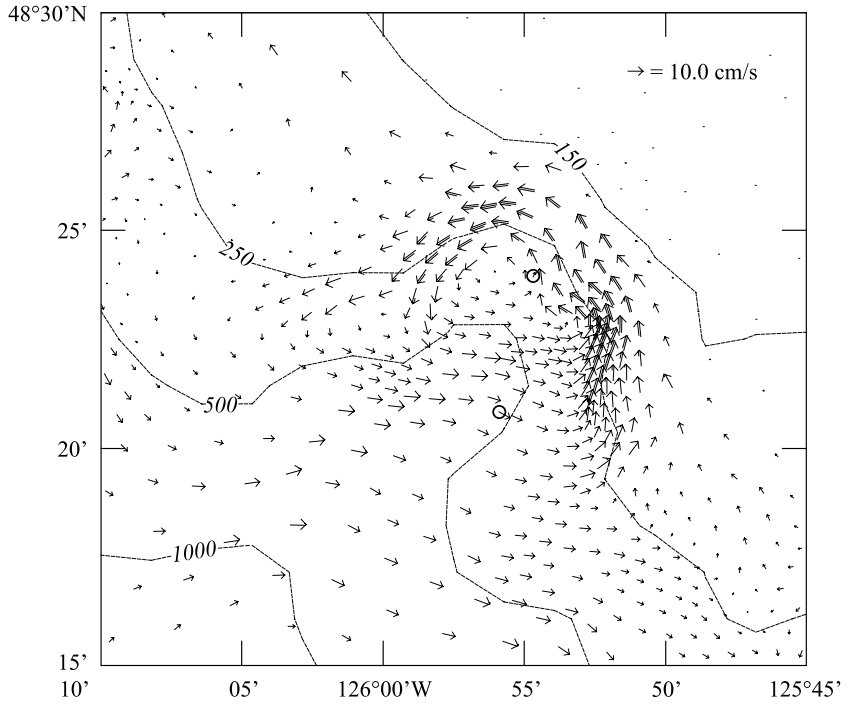

Figure 14. Currents over Barkley Canyon at 150 m depth. Currents were found from inverting the density field using a diagnostic model. The currents in circles are two current meter measurements from the same time. (After Allen et al., 2001.)

flow over the canyon by a purely oscillatory flow is an illustration of the strength of asymmetry between upwelling and downwelling over a canyon. As upwelling is stronger, oscillatory flow drives net upwelling in the canyon. Using Barkley Canyon geometry for reference, the mean flow generated includes a cyclonic eddy within and toward the North edge of the canyon and an anti-cyclonic eddy at the mouth to the South. Over Barkley Canyon, however, these rectified flows are expected to be small due to the small tidal excursion compared to the canyon width.

2.6. Effects on biology

Current meter observations above 150 m were not collected above Barkley Canyon in 1997 but the diagnostic model forced by observed density fields showed only weak deflections of the currents over the canyon, consistent with numerical predictions and previous observations (Allen et al., 2001). The CTD observations, however, show near-surface effects in the form of a strongly raised seasonal thermocline (Figure 15) that is neither predicted

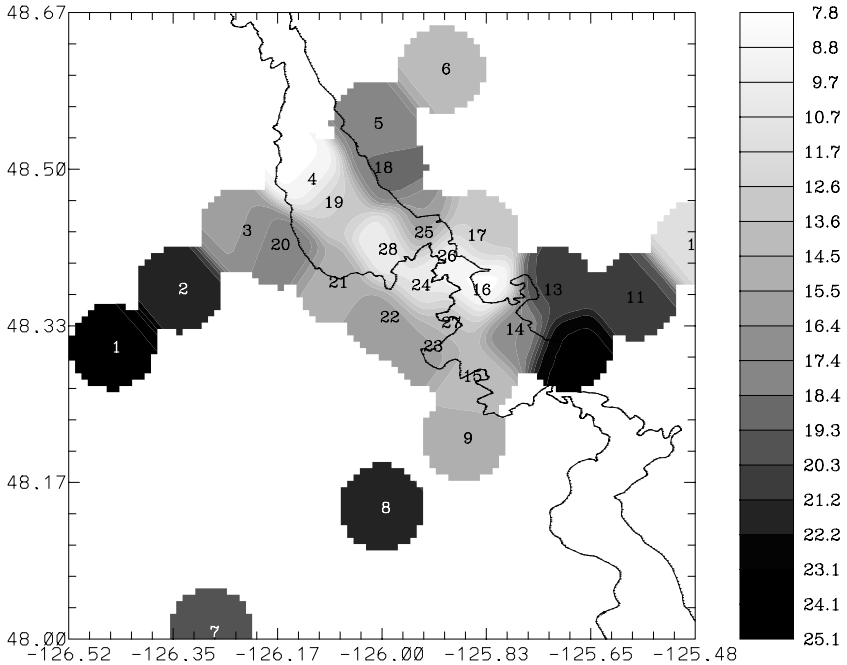

Figure 15. Depth of the 24 sigma-*t* density surface over Barkley Canyon, July 1997. This surface occurs in the seasonal pycnocline and shows the lifting of the pycnocline over the canyon and shelf-break (light shading). The two isobaths shown are the 200 and 300 m. The numbers show the order of sampling. After Allen et al. (2001).

by the prognostic numerical models nor observed over Astoria Canyon (Hickey, 1997). The surface layer containing high particulate concentration is thinned by the raised thermocline. As the depth of the thermocline is halved over the canyon, the raised thermocline could significantly increase the rate of entrainment into the mixed layer above. Also water below the thermocline would be raised into the euphotic zone. Both processes should act to raise euphotic zone nutrient availability and phytoplankton productivity at the shelf-break and over the canyon.

Nutrients were sampled at stations 1–12 (Figure 15). Nutrients at station 4 at the shelf-break where the thermocline is raised were neither anomalously high nor associated with increased chlorophyll levels. The lack of a definitive canyon-induced nutrient anomaly for this canyon is probably due to the overriding effect of strong coastal nutrient input from the nearby Vancouver Island Coastal Current and regional coastal upwelling (Figure 5).

2.6.1. Zooplankton

Zooplankton distributions (shallow versus full water column, and daylight versus night) were compared among four stations around Barkley Canyon by Allen et al. (2001). Two of the stations were close to the walls at the mouth of the canyon, and the last two were at the head of the canyon on the shelf. For each pair, one was on the North side (upstream) and the other downstream. The basic sampling design was a set of four bongo vertical net tows at each of these sites: one visit during daylight and one during the night, and, at each visit, one shallow tow from 50 m to the surface and one deep tow (from 250 m to the surface at the two deeper sites, from approximately 15 m above the bottom to the surface at the shallower sites). The taxa selected for analysis included species that were dominant within the local zooplankton community during the preceding decade (Mackas, 1992) but were also selected to include a range of body size, migratory strategy, and shelf versus oceanic primary habitat. The species were divided into groups based on three criteria: (1) Their usual cross-shore location in the southern section of the Vancouver Island continental margin (shelf, shelf-edge or oceanic); (2) whether they usually follow a diel migration pattern (migrators or non-migrators); and (3) whether they were found predominantly above or below 50 m (shallow, deep or mixed). For each species at each time (day or night) and for each depth of tow, the number of animals per square meter was calculated by dividing the total catch per sample by the volume filtered (from the flow meter), and then multiplying by the vertical range of the tow.

Species that were found only in the upper 50 m depth stratum both day and night were generally found at the same cross-shore location over the canyon as they are in other places along the southern shelf (as sketched in

Figure 16). Species found deeper (not including euphausiids) were found to be shifted shoreward by about the length of the canyon (as sketched in Figure 17) (Allen et al., 2001). Thus, except for the euphausiids, the observed zooplankton distribution of all major species was consistent with passive advection by the currents.

The larger bodied, strongly migratory adults and late juveniles of both euphausiid species *Euphausia pacifica* and *Thysanoessa spinifera* were most abundant in the eddy region, near the head of the canyon. This in-canyon similarity of distribution is an interesting result, because their larger scale distributions are quite different. Specifically, *T. spinifera* is a shelf species while *E. pacifica* is a shelf break-oceanic species.

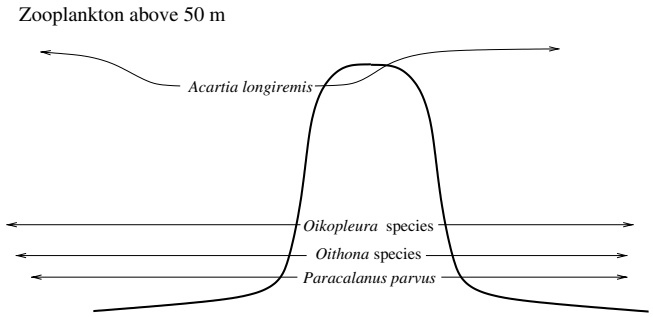

Figure 16. Sketch of the distribution of zooplankton above 50 m depth over Barkley Canyon, July 1997. The line without arrows represents the rim of the canyon. The normal position of the species is shown away from the canyon and the observed distribution is shown over the canyon.

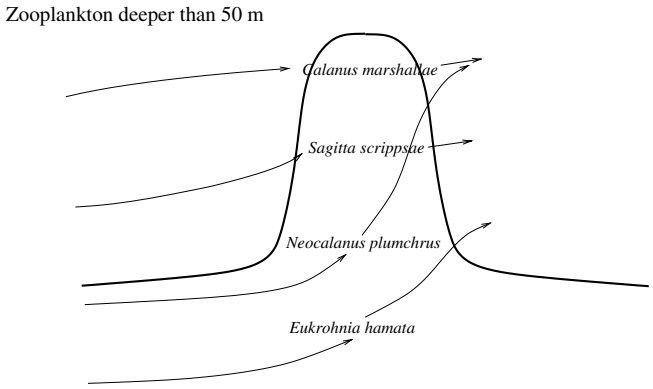

Figure 17. Sketch of the distribution of zooplankton below 50 m depth excluding euphausiids over Barkley Canyon, July 1997. The line without arrows represents the rim of the canyon. The normal position of the species is shown away from the canyon and the observed distribution is shown over the canyon.

As the eddy is 10 km wide compared to the tidal excursion of 0.9 km, and has current speeds of 20 cm s^{-1}, as compared to the barotropic tidal current of 2 cm s^{-1}, it is expected to trap tracers (at 150 m) in a Lagrangian sense (Foreman et al., 1992). Eddies and other recirculating flows can trap passive tracers but do not aggregate them. However, the euphausiid species *Euphausia pacifica* and *Thysanoessa spinifera* were observed to be aggregated in the eddy region (Allen et al., 2001). Although flow in the ocean is non-divergent in three dimensions, there can be regions of horizontal convergence (divergence). As the euphausiids can maintain their preferred depth against the weak vertical velocities they can be aggregated by horizontal convergence. An example is given in Mackas et al. (1997) where euphausiids are seen to aggregate in regions of strongly sloping bottom topography due to flow toward the slope. Regions of strong convergence are seen at depths occupied by euphausiids during the day. Euphausiids have been shown to aggregate at the shelf-edge upstream of the canyon at about 100 m depth (Mackas et al., 1997). Very strong regions of convergence occur particularly in the region where the eddy flow crosses the downstream rim (Allen et al., 2001). Only zooplankton caught at the eddy station passed through a convergence zone just before being trapped.

3. Spin-up over realistic topography

3.1. Classic Spin-up

Consider a cylindrical laboratory tank sitting on a rotating table, rotating in solid body rotation with rotation rate $(f - \Delta f)/2$. The tank contains homogeneous water. If the rotation rate of the table is increased to $f/2$, the tank will follow the table but the water in the tank will continue to rotate at its original rate. In the frame of the rotating table, the fluid will flow clockwise at approximately $\Delta f r/2$, where r is the radius from the centre of the tank. An Ekman layer will form at the bottom of the tank with depth $\delta = (2\nu/f)^{1/2}$ where ν is the kinematic viscosity. In the Ekman layer the flow is radially outward with a mass flux of δu_θ where u_θ is the azimuthal velocity above the boundary layer. As the flow in the tank has vorticity, the mass flux in the Ekman layer has divergence. This divergence causes Ekman pumping into the Ekman layer. The Ekman pumping stretches the fluid columns above, reducing their negative vorticity (Figure 18). The water in the tank quickly reaches the new rotation rate in a time Hf/δ where H is the depth of the tank. For a typical laboratory tank apparatus, $H \approx 10$ cm, $f \approx 0.5$ s^{-1} and thus $\delta = 2$ mm and the spin-up time is 1000 s or about 17 min.

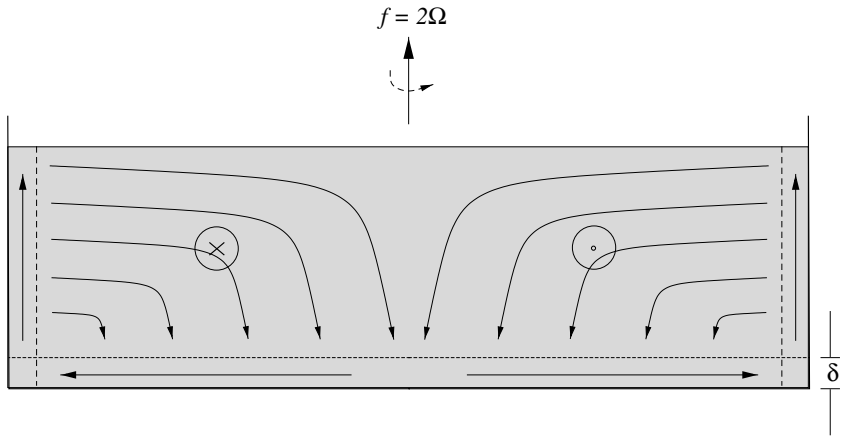

Figure 18. Sketch of the flow pattern for homogeneous spin-up in a cylindrical tank with a free surface. After Mirshak (2001).

3.2. Stratified Spin-up

Consider again the cylindrical tank with a flat bottom, but now with a stratified fluid in the tank. The large scale vertical motions illustrated in Figure 18 are suppressed by the stratification. The secondary circulation is restricted in the vertical and occupies a depth fR/N where R is the radius of the tank and N is the Brunt–Väisälä or buoyancy frequency (Figure 19).

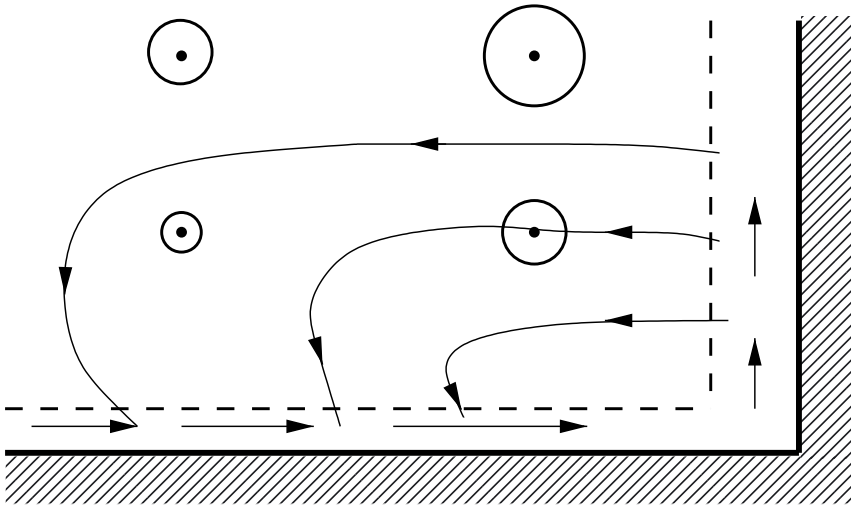

Figure 19. Schematic of stratified flow over a flat bottom.

As a smaller region of the flow participates in the spin-up, the spin-up is faster in this region. Above this flow, the flow continues at the old rotation rate and is only spun-up by vertical and horizontal diffusion of momentum. This process is much slower than Ekman spin-up. For 10 cm of water above the spun-up fluid, the diffusion time-scale is 1.0×10^4 s or 2.8 h.

3.3. Stratified Spin-up on a slope

Consider now flow over a slope. If the fluid is homogeneous, the Ekman layer is little changed (Pedlosky, 1979). The Ekman layer thickness is $\delta_s = (2\nu/f\cos\alpha)^{1/2}$ where α is the slope. The Ekman spiral is identical except for the slight change in the boundary layer thickness. The flux along the slope becomes $\delta_s u_\theta$ which is slightly bigger than for the flat bottom case. However the radial velocity remains unchanged.

However, if the flow is stratified, the presence of a slope strongly changes the flow pattern. The Ekman layer initially generated over the slope causes upslope flow which advects denser water up the slope. This dense water causes a buoyancy force parallel to and down the slope. In this direction,

$$\frac{\partial u_r}{\partial t} - f u_\theta = \frac{-1}{\rho_o}\frac{\partial p}{\partial r} - \frac{1}{\rho_o}\frac{\partial p'}{\partial r} + \nu\frac{\partial^2 u_r}{\partial z^2} \tag{5}$$

where u_r is the upslope velocity, u_θ is the along slope velocity, $\partial p/\partial r$ is the background pressure gradient driving the geostrophic velocity above the boundary layer and $\partial p'/\partial r$ is the pressure gradient generated by the dense water advection

$$\frac{\partial p'}{\partial z} = -\rho' g \tag{6}$$

where ρ' is the density change. At some point the pressure gradient can become large enough to balance the background pressure gradient. After this time, there will be no velocity at the bottom (a thermal wind balance with zero velocity near the bottom) and so no further advection of fluid up the slope. (Ignoring diffusion of density, which is applicable for salt in the laboratory). Thus all further velocity modifications will be due to viscosity (Figure 20).

Assuming that initially an Ekman layer forms on the slope, upslope velocity within the Ekman layer is proportional to the geostrophic velocity U_g. Thus the density rate of change

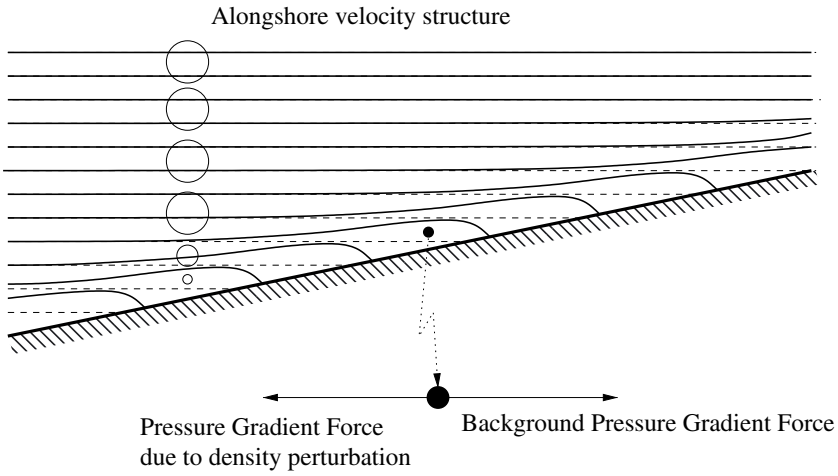

Figure 20. Isopycnal deflection due to upslope Ekman transport; the eventual pressure balance and along-slope thermal wind velocity structure. Note that the thickness of the boundary layer will increase in time due to diffusion until the whole flow reaches zero velocity.

$$\frac{\partial \rho'}{\partial t} = \frac{\rho_o U_{\mathrm{g}} \tan \alpha N^2}{g} \tag{7}$$

and so scaling the hydrostatic equation the vertical perturbation pressure gradient is approximately

$$\frac{\partial p'}{\partial z} = \rho_o U_{\mathrm{g}} \tan \alpha N^2 t \tag{8}$$

where t is the time. The horizontal pressure gradient is

$$\frac{\partial p'}{\partial r} = \rho_o U_g \tan \alpha N^2 t \sin \alpha \tag{9}$$

The background pressure gradient is $\rho_o f U_{\mathrm{g}}$, equating gives

$$t = \frac{f \cos \alpha}{N^2 \sin^2 \alpha} \tag{10}$$

which is an underestimate for the shut-down time for the Ekman layer. A full time-dependent derivation gives

$$\tau_{\mathrm{s}} = \frac{1}{Sf \cos \alpha (1 + S)} \tag{11}$$

where $S = (N \sin\alpha / f \cos\alpha)^2$ (MacCready and Rhines, 1991).

Once the Ekman layer has reached approximate thermal wind balance, the cross-slope momentum balance is approximately

$$-fu_\theta \approx \frac{-1}{\rho_o}\frac{\partial p}{\partial r} - \frac{1}{\rho_o}\frac{\partial p'}{\partial r} \tag{12}$$

where $\partial p'/\partial r = \rho' \tan\alpha$ and $\partial \rho'/\partial t = N^2 \tan\alpha u_r/\rho_o$. Combining and substituting into the along-slope momentum equation gives (Mirshak, 2001):

$$\frac{\partial u_\theta}{\partial t}(1+S) = \nu\left(\frac{\partial^2 u_\theta}{\partial z^2} + \frac{\partial^2 u_\theta}{\partial r^2}\right) \tag{13}$$

This equation is equivalent to that of MacCready and Rhines (1991) with the addition of diffusion in the radial direction.

3.4. Spin-up over realistic topography

Now consider spin-up over a more realistic topography; that is, a shelf, shelf-break, slope, deep-ocean topography inserted into a laboratory tank (Figure 21).

Consider the case where the tank initially rotates at a speed $f = 0.4\ \mathrm{s}^{-1}$ and then the speed of the table is increased, over 1 inertial period (23 s) to $f = 0.52\ \mathrm{s}^{-1}$. For a stratification of $N = 2.2\ \mathrm{s}^{-1}$ the shut-down time for the

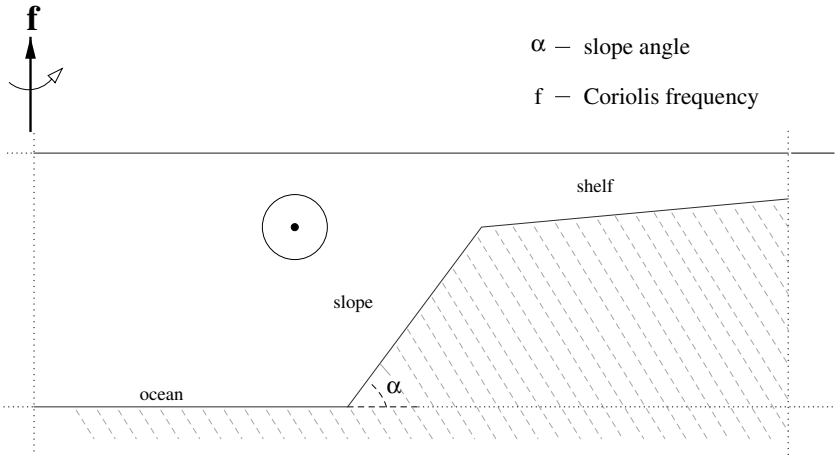

Figure 21. Sketch showing shelf/slope/deep-ocean topography for a cylindrical tank. The tank rotates around the centre as shown. Flow is forced by changing the rotation rate of the tank. (After Mirshak, 2001.)

Ekman layer is 20 s over the shelf. So over the shelf both regimes: the initial Ekman layer and Ekman suction regime (dominates for the first 20 s) and the shutdown Ekman layer and diffusion regime (dominates after 20 s) will be observed.

Combining Ekman layer suction decreasing exponentially with the spin-up time ($\exp(-t/\tau_s)$) and diffusion as specified in (13) one can numerically solve for the spin-up in a stratified fluid over complicated topography (Mirshak, 2001). Not surprisingly spin-up in the shallow water occurs quickly whereas the deep water and water over the slope continue to flow well into the experiment. A comparison of the approximate numerical solution to the observations shows good agreement (Figure 22).

3.5. Effect of a canyon

In a stratified fluid for realistic topography spin-up time is greatly increased because the Ekman layers shut-down. What if the topography is not axially symmetric? What if we introduce a small canyon (Figure 23)? Now the problem looks a little like canyon upwelling. We have a flow (in the opposite direction to Kelvin wave propagation) along the shelf, over a canyon. We expect flow up the canyon as explained in the previous section. This flow can take the place of flow in the Ekman layers and continue after the Ekman layers are shut-down. Thus we expect enhanced spin-up.

If there is no canyon we can predict (using the numerical model above) how the flow will evolve. This prediction can be compared to the observations with a canyon to separate the canyon effect (Figure 24).

If one considers the total flow in the annulus over the shelf the extra decrease in velocity with the canyon present is equal to the drag caused by the canyon.

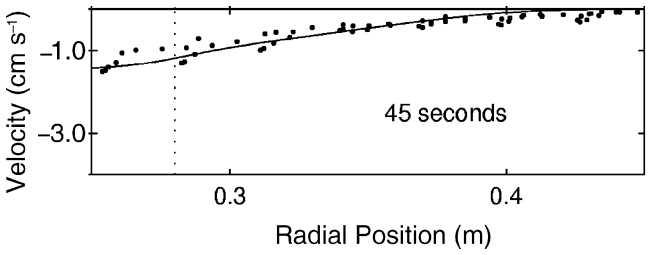

Figure 22. Velocity in the tank as a function of radius. The centre of the tank is at 0 m, the shelf break is the dotted line and the edge of the tank is at 0.5 m. Dots are observations. The line is the numerical result 45 s after the table acceleration. The initial value for the numerical simulation was taken for observations 0 s after the table acceleration. After Mirshak (2001).

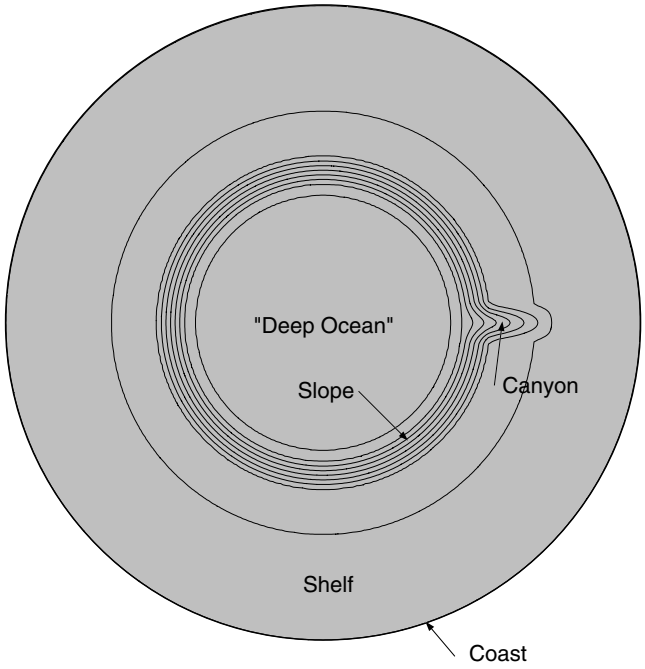

Figure 23. Schematic bathymetric map of the topography in the bank. Contours are 1 cm apart. The vertical scale is exaggerated compared to the horizontal scale by a factor of 10 (radius of tank is 50 cm). The ''shelf'' slope is 5° and the ''slope'' slope is 45°. From Allen et al. (2003).

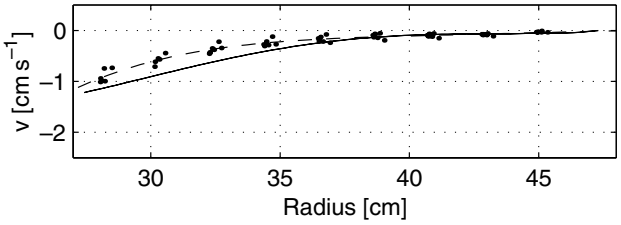

Figure 24. Solid line shows prediction assuming no canyon. Dots are observations with a canyon. Dashed line is a fit to the observations. Reprinted with permission from Mirshak (2001).

$$F_{\text{drag}} = -\Delta \frac{\partial u_\theta}{\partial t} V \tag{14}$$

where V is the volume of the annulus. Here the Coriolis force on the radial velocity has been neglected because averaged over the whole annulus the radial velocity is zero. From laboratory data it is found (Mirshak, 2001) that

$$F_{\text{drag}} = \mathcal{O}\left(U^2 f^{0.5}/N\right). \tag{15}$$

If one considers just the fluid in the canyon the flow is to first order geostrophic and the form drag is balanced by a flux up the canyon.

$$F_{\text{drag}} = f u_r \tag{16}$$

where in the vicinity of the canyon the time rate of change of the alongshore flow is neglected. Combining this equation with the drag equation allows the flux up the canyon to be calculated (Mirshak, 2001). From the canyon scaling part of the previous section we had a scale for the upwelling flux $\Phi = Z U_s W_{sb}$ where Z is the depth of upwelling, U_s is the velocity of the upwelling stream and W_{sb} is the width of the canyon. A comparison gives the coefficient for upwelling flux as 0.95 (Figure 25).

3.6. Implications

From the estimate of the upwelling flux from the canyon, we can apply the formula to the real ocean. Considering the southern coast of Vancouver Island, three short canyons cut the shelf-break. These three canyons produce (in some years) almost as much summer upwelling as the direct wind driven upwelling. For example, in 1998, the summer (May–August) canyon upwelling is estimated as 1.9×10^5 Sv s versus 1.8×10^5 Sv s for wind-driven upwelling (Mirshak et al., 2002).

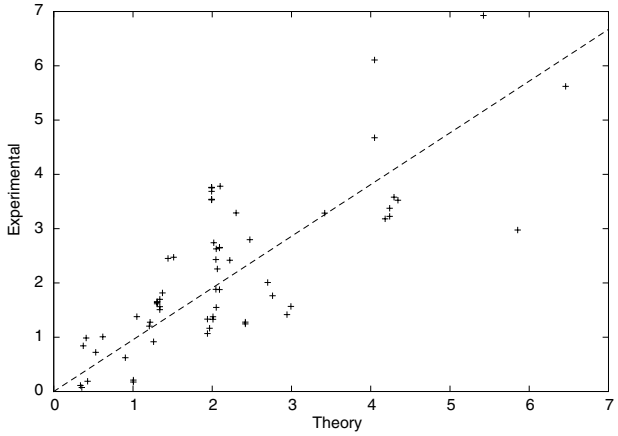

Figure 25. Comparison between upwelling theory and the experimental estimate for flux through the canyon in $cm^3\ s^{-1}$. The gradient of the best fit line is 0.95.

4. Future directions

This manuscript has considered only short canyons. Canyons that reach all the way to the coast are expected to have a much stronger effect on upwelling. In particular, Juan de Fuca Canyon generates strong, summer long upwelling (Allen, 2000). These canyons deserve further study as a strong conduit for deep flow across the shelf-break.

References

Allen, S. E.: 2000, 'On Subinertial Flow in Submarine Canyons: Effect of Geometry', *J. Geophys. Res.* **105**, 1285–1297.

Allen, S. E., Dinniman, M. S., Klinck, J. M., Hewett, A., and Hickey, B. M.: 2003, 'On Vertical Advection Truncation Errors in Terrain Following Numerical Models: Comparison to a Laboratory Model for Upwelling over Submarine Canyons', *J. Geophys. Res.* **108**, 3003, doi 10.1029/2001JC000978.

Allen, S. E., Vindeirinho, C., Thomson, R. E., Foreman M. G. G., and Mackas, D. L.: 2001, 'Physical and Biological Processes Over a Submarine Canyon During an Upwelling Event', *Can. J. Fish. Aquat. Sci.* **58**, 671–684.

Boyer, D. L., Zhang X., and Perenne, N.: 2000, 'Laboratory Observations of Rotating, Stratified Flow in the Vicinity of a Submarine Canyon', *Dyn. Atmos. Oceans*, **31**: 47–72.

Cushman-Roisin, B.: 1994, *Introduction to Geophysical Fluid Dynamics*, Prentice Hall.

Eurin, D.: 1999, *Circulation and Cross-shelf Exchanges over an Irregular Coastal Topography*, Masters thesis, University of British Columbia.

Foreman, M. G. G., Bapista, A. M., and Walters, R. A.: 1992, 'Tidal Model Studies of Particle Trajectories Around a Shallow Coastal Bank'. *Atmos. -Ocean*, **30**, 43–69.

Freeland, H. J., and Denman, K. L.: 1982, 'A Topographically Controlled Upwelling Center Off Southern Vancouver Island', *J. Mar. Res.* **40**, 1069–1093.

Harris, S.: 2001, *Size-fractionated Chlorophyll and Primary Productivity and Nutrient Distributions Off the West Coast of Vancouver Island*, Masters thesis, University of British, Columbia.

Hickey, B. M.: 1997, 'The Response of a Steep-Sided Narrow Canyon to Strong Wind Forcing', *J. Phys. Oceanogr.* **27**, 697–726.

Hogg, N. G.: 1973, 'On the Stratified Taylor Column', *J. Fluid Mech.* **58**, 517–537.

MacCready, P., and Rhines, P. B.: 1991, 'Buoyant Inhibition of Ekman Transport on a Slope and its Effect on Stratified Spin-up', *J. Fluid Mech.* **223**, 631–661.

Mackas, D. L.: 1992, 'Seasonal Cycle of Zooplankton Off Southwestern British Columbia', *Can. J. Fish. Aquat. Sci.* **49**, 903–921.

Mackas, D. L., Kieser, R., Saunders, M., Yelland, D. R, Brown, R. M., and Moore, D. F.: 1997, 'Aggregation of Euphasiids and Pacific Hake (*Merluccius productus*) along the Outer Continental Shelf Off Vancouver Island', *Can. J. Fish. Aquat. Sci.* **54**, 2080–2096.

Mirshak, R.: 2001, *Spin-up Over Steep Topography and the Effects of a Submarine Canyon*, Masters thesis, University of British Columbia.

Mirshak, R., Allen, S.E., Thomson R.E., and Waterhouse A.: 2002, 'Submarine Canyon Upwelling Off the West Coast of Vancouver Island, Canada (Abstract)', *EOS Trans.* **83** Supplement.

Pedlosky, J.: 1979, *Geophysical Fluid Dynamics*, Springer-Verlag.